Routes to chaos in a class-B laser coupled to a neutral resonator

L. E. Güemes Frese,[1,*] B. R. Jaramillo-Ávila,[2,†] and B. M. Rodríguez-Lara[1,‡]
[1]*Tecnologico de Monterrey, Escuela de Ingeniería y Ciencias, Ave. Eugenio Garza Sada 2501, Monterrey, N.L., Mexico, 64849*
[2]*CONACYT - Instituto Nacional de Astrofísica, Óptica y Electrónica, Calle Luis Enrique Erro No. 1. Sta. Ma. Tonantzintla, Pue. C.P. 72840, Mexico*

(Received 22 April 2022; accepted 15 August 2022; published 12 September 2022)

We study the dynamics of a class-B semiconductor microring laser coupled to a neutral microring resonator for common fabrication parameters. For zero detuning between the resonators, we identify five dynamical regions controlled by the laser pump parameter above threshold and the coupling strength between the resonators. These regions show stable lasing with phase locking for either sufficiently small or large coupling strength parameter values. Multistability and chaos arise in between these stable regions where at least one fixed point is attractive. The transition from stable to unstable lasing regions in the parameter space phase diagram is a crossover.

DOI: 10.1103/PhysRevA.106.033507

I. INTRODUCTION

Arrays of coupled semiconductor microring lasers are of both technological and fundamental importance in optics. They may be engineered to emit in synchronization, producing a coherent light source where the power of several microrings is added [1,2]. Coupled in specific configurations, these arrays may harbor topological effects, such as edge states [3–7], or may exhibit dynamic instabilities that lead to chaos. While seemingly undesirable, chaos synchronization in these systems enables secure communications, for example, chaos-based cryptography [8–12].

The most common type of semiconductor laser is the class-B laser [5,13,14]. Its mathematical model arises from Maxwell-Bloch equations in the limit where the lifetime of the active medium polarization is much shorter than the lifetime of both carriers in the media and photons in the cavity [13,15]. A single class-B laser by itself produces a stable field and, therefore, does not lead to dynamic instabilities or chaos. When several class-B lasers are coupled, the array can display synchronization [16,17], cluster synchronization [18], and chaos and chaos chimeras [19,20]. These effects are relevant for coherent emission [1,2], topological states [3–7], and chaos-based encryption [11,12].

The dynamical behavior of coupled arrays of identical [16,17] and nonidentical [21] class-B lasers has been elucidated in the literature. Laser arrays are often built by repeating a unit cell formed by a few coupled semiconductor lasers. Understanding the behavior of these unit cells is necessary to describe the larger arrays. The unit cell formed by a pair of coupled microring lasers pumped at different rates has been extensively studied. It displays nonlinear dynamics similar to those of a non-Hermitian $\mathcal{PT}$ dimer [22] that displays limit cycles and tunability [23], phase synchronization [23–25], and bifurcations and chaos [26–28]. Arrays formed by coupling copies of this differentially pumped cell enable novel topological and collective effects [5–7,29].

Here, we focus on a class-B microring semiconductor laser coupled to a passive microring. This simple unit cell produces equivalent dynamics to the gain-loss dimer and shows dynamical instabilities and chaos even if a single class-B laser does not. The passive microring has an effect similar to coupling a mirror to the laser, which introduces time-delay effects and leads to dynamical instabilities [30,31], however, our model is free from explicit time delays. In Sec. II, we provide a brief review of the dynamics in a single class-B laser. Next, we present our model, and study its fixed points and the phase diagram provided by its parameters in Sec. III; we focus on the zero detuning case and find two fixed points, one where the phases of the microrings are synchronized and one where they differ by half a cycle. In Sec. IV, we characterize the parameter regions where these fixed points are stable, leading to stable synchronization and antisynchronization. We also explore the parameter values where dynamical instabilities and chaos arise. Finally, in Sec. V, we close with our conclusions.

II. SINGLE CLASS-B LASER

To provide context, we present a brief review of the dynamics in a single class-B laser [13,14,32],

$$i\dot{\mathcal{E}}(t) = \frac{i(1-i\alpha)}{2}\left\{-\frac{1}{\tau_p} + \sigma[n(t)-1]\right\}\mathcal{E}(t), \tag{1}$$

$$\dot{n}(t) = R - \frac{n(t)}{\tau_s} - \frac{2[n(t)-1]}{\tau_s}|\mathcal{E}(t)|^2, \tag{2}$$

in terms of the complex amplitude of the resonant electric field mode $\mathcal{E}(t)$ and the carrier density normalized to transparency $n(t)$. The parameters of the model are the linewidth enhancement factor α, carrier lifetime τ_s, cavity lifetime τ_p, differential gain σ, and normalized pump rate R. We may safely assume that in any given experimental realization, the carrier lifetime is larger than the cavity lifetime which in turn

*a01154875@tec.mx
†jaramillo@inaoep.mx
‡bmlara@tec.mx

TABLE I. Fixed-point classification from the stability analysis of a single class-B laser.

Region	$(I^{(1)}, N^{(1)})$	$(I^{(2)}, N^{(2)})$
$P < P^{(A)}$	Sink or node (type I), stable	Saddle point
$P^{(A)} < P < P^{(B)}_{-}$	Saddle point	Sink or node (type I), stable
$P^{(B)}_{-} < P < P^{(B)}_{+}$	Saddle point	Spiral sink, stable
$P^{(B)}_{+} < P$	Saddle point	Sink or node (type I), stable

is larger than the inverse differential gain, $\tau_s \gg \tau_p \gg \sigma^{-1}$ [14,15]. For the sake of simplicity, we move into the frame,

$$\frac{d}{ds}I(s) = N(s)I(s), \tag{3}$$

$$\frac{d}{ds}N(s) = \gamma\{P - N(s) - [N(s)+1]I(s)\}, \tag{4}$$

provided by the dimensionless time $s = t/\tau_p$, twice the squared absolute value of the field mode amplitude $I(s) = 2|\mathcal{E}(s)|^2$, that allows us to uncouple the dynamics of phase, and a new carrier parameter $N(s) = \sigma\tau_p[n(s)-1]-1$, that is related to the carrier density normalized to transparency. Additionally, two new constants are introduced, the cavity to carrier lifetime ratio $\gamma = \tau_p/\tau_s$ and the pump parameter above threshold $P = \sigma\tau_p(\tau_s R - 1) - 1$. This frame allows us to find two fixed points,

$$I^{(1)} = 0, \quad N^{(1)} = P, \tag{5}$$

$$I^{(2)} = P, \quad N^{(2)} = 0. \tag{6}$$

A standard stability analysis of the system requires the eigenvalues of the Jacobian,

$$\lambda^{(j)}_{\pm} = -\frac{1}{2}\left[\gamma(I^{(j)}+1) - N^{(j)}\right] \pm \frac{1}{2}\sqrt{[\gamma(I^{(j)}+1) - N^{(j)}]^2 + 4\gamma(N^{(j)} - I^{(j)})}, \tag{7}$$

evaluated at each fixed point, where $j = 1, 2$, to understand the dynamics in the neighborhood of that point [33,34].

The fixed points and Jacobian eigenvalues lead to various critical values of the pump parameter above threshold. Among these, three are crucial,

$$P^{(A)} = 0, \tag{8}$$

$$P^{(B)}_{\pm} = -1 + \frac{2}{\gamma} \pm \frac{2}{\gamma}\sqrt{1-\gamma}. \tag{9}$$

The first one corresponds to the critical pump parameter above threshold where the absolute value of the field amplitude at the second fixed point becomes non-negative, and therefore physical. Above that value, $P^{(A)} < P$, the second fixed point is stable. There, for all physical initial conditions the system evolves to stable nonzero values for both the squared absolute value of the field amplitude and carrier parameter. These values are provided by the second fixed point $(I^{(2)}, N^{(2)})$. For values of the pump parameter below it, $P < P^{(A)}$, neither fixed point has finite and stable field amplitudes; in fact, the first fixed point $(I^{(1)}, N^{(1)})$ always has vanishing field amplitude. Below this value, for all physical initial conditions the system evolves to zero-field amplitude and carrier parameter to a negative value equal to $N = P$. The latter is smaller than the stable carrier parameter when the laser is pumped above the threshold. The other pair of critical values of the pump parameter above threshold, $P^{(B)}_{\pm}$, arise from evaluating the Jacobian at the second fixed point and finding the values where the Jacobian eigenvalues acquire or lose an imaginary part. At these critical values of the pump parameter above threshold $P^{(B)}_{\pm}$, the fixed point acquires or loses spiral behavior. Under the hierarchy $\tau_s \gg \tau_p \gg \sigma^{-1}$, these critical rates organize themselves,

$$P^{(A)} < P^{(B)}_{-} < P^{(B)}_{+}, \tag{10}$$

in a manner that highlights four regions leading to a classification of the fixed points (Table I). Thus, we observe lasing once the pump parameter above threshold reaches the threshold value of zero, $P_{\text{th}} = P^{(A)}$. After this threshold value, the second fixed point $(I^{(2)}, N^{(2)})$ behaves as a stable sink in the region $P_{\text{th}} < P < P^{(B)}_{-}$, then as a stable spiral sink in the region $P^{(B)}_{-} < P < P^{(B)}_{+}$, and, finally, as a stable sink after that, $P^{(B)}_{+} < P$ [13,32].

III. CLASS-B LASER COUPLED TO A NEUTRAL RESONATOR

An usual path to chaos in class-B lasers is to induce feedback by introducing an external mirror [30,31]. Here, we want to study the dynamics of a class-B laser interacting with a neutral resonator under minimal coupling [35,36],

$$i\dot{\mathcal{E}}_1(t) = \frac{i(1-i\alpha)}{2}\left\{-\frac{1}{\tau_p} + \sigma[n(t)-1]\right\}\mathcal{E}_1(t) + \omega_1\mathcal{E}_1 + g\mathcal{E}_2(t), \tag{11}$$

$$i\dot{\mathcal{E}}_2(t) = \omega_2\mathcal{E}_2(t) + g\mathcal{E}_1(t), \tag{12}$$

$$\dot{n}(t) = R - \frac{n(t)}{\tau_s} - \frac{2[n(t)-1]}{\tau_s}|\mathcal{E}_1(t)|^2, \tag{13}$$

where we define the complex amplitudes $\mathcal{E}_j(t)$ of the electric field modes localized at each resonator, its corresponding resonant frequency ω_j, and the coupling strength between them g. Moving into a frame rotating at the resonant frequency of

TABLE II. Fixed-point classification from the stability analysis of a class-B laser coupled to a neutral resonator.

Region	$(I_1^{(1)}, I_2^{(1)}, \varphi^{(1)}, N^{(1)})$	$(I_1^{(2)}, I_2^{(2)}, \varphi^{(2)}, N^{(2)})$
Region I	Saddle point	Saddle point
Region II	Saddle point	Sink or spiral sink, stable
Region III	Sink or spiral sink, stable	Sink or spiral sink, stable
Region IV	Sink or spiral sink, stable	Saddle point
Region V	Saddle point	Saddle point

the laser,

$$\mathcal{E}_j(t) = \sqrt{I_j(t)/2}\exp[i\phi_j(t)], \tag{14}$$

and rewriting the differential equation set,

$$\frac{d}{ds}I_1(s) = N(s)I_1(s) - 2g\tau_p\sqrt{I_1(s)I_2(s)}\sin\varphi(s), \tag{15}$$

$$\frac{d}{ds}I_2(s) = 2g\tau_p\sqrt{I_1(s)I_2(s)}\sin\varphi(s), \tag{16}$$

$$\frac{d}{ds}\varphi(s) = \Delta\omega\tau_p - \frac{\alpha}{2}N(s) + g\tau_p\frac{I_1(s)-I_2(s)}{\sqrt{I_1(s)I_2(s)}}\cos\varphi(s), \tag{17}$$

$$\frac{d}{ds}N(s) = \gamma\{P - N(s) - [N(s)+1]I_1(s)\}, \tag{18}$$

using the dimensionless time $s = t/\tau_p$, the detuning between the resonator frequencies $\Delta\omega = \omega_2 - \omega_1$, twice the squared amplitudes $I_j(s) = 2|\mathcal{E}_j(s)|^2$, the carrier parameter $N(s) = \sigma\tau_p[n(s)-1]-1$, and the phase difference $\varphi(s) = \phi_1(t) - \phi_2(s)$, we find four fixed points,

$$\left\{\left(I_1^{(j)}, I_2^{(j)}, \varphi^{(j)}, N^{(j)}\right)\right\}, \tag{19}$$

with $j = 1, 2, 3, 4$, arising from the combination of the two sign options for the square root in the squared absolute value of the field amplitude inside the neutral resonator $I_2^{(j)}$ and the two phase difference options $\varphi^{(j)}$,

$$I_1^{(j)} = P, \tag{20}$$

$$I_2^{(j)} = \frac{1}{2g^2}\left(2g^2 + \Delta\omega^2 \pm \Delta\omega\sqrt{4g^2+\Delta\omega^2}\right)P, \tag{21}$$

$$\varphi^{(j)} = 0, \pi, \tag{22}$$

$$N^{(j)} = 0. \tag{23}$$

It is straightforward to notice that the case of microrings with identical resonator frequencies, $\Delta\omega = 0$, reduces to just two fixed points with an equal squared absolute value of the field amplitudes, $I_2^{(j)} = I_1^{(j)}$. For the sake of simplicity, we focus our analysis on this case.

For this zero detuning case, $\Delta\omega = 0$, the squared absolute value of the field amplitudes at either fixed point is negative and therefore unphysical, unless the pump parameter is above a threshold value of zero,

$$P_{\text{th}} = 0, \tag{24}$$

identical to that of the single class-B laser. This threshold depends only on the gain-resonator parameters and is not influenced by the coupling to the neutral resonator. Again, the system will not lase if the pump parameter P is below zero, Region I in Table II and Fig. 1(a) where both fixed points are saddle points. However, the behavior above the lasing threshold is richer. We find one stable fixed point in regions II and IV, and two of them in region III. These should provide us with stable lasing. In region V, both fixed points behave as saddle points and chaos arises [33,34]. In the following, we address with more detail the dynamics of our model in these five regions.

IV. PARAMETER SPACE PHASE DIAGRAM

Our dynamical system displays two fixed points in the zero detuning case, $\Delta\omega = 0$. We use a standard stability analysis [33,34] to find the parameter values where these fixed points become attractive, pulling nearby trajectories. This leads to stable behavior of the system for configurations (I_1, I_2, φ, N) at and near the fixed point. To do this, we use typical class-B laser parameters $\alpha = 3$, $\tau_s = 4$ ns, $\tau_p = 40$ ps, and $\sigma^{-1} = 1.67$ ps [5], and couplings ranging from zero to a few tens of inverse nanoseconds [6,7]. Figure 1 displays the regions defined by the dynamical characteristics nearby the two fixed points. This parameter space phase diagram depends on the pump parameter above threshold P and the coupling strength g and contains five different regions.

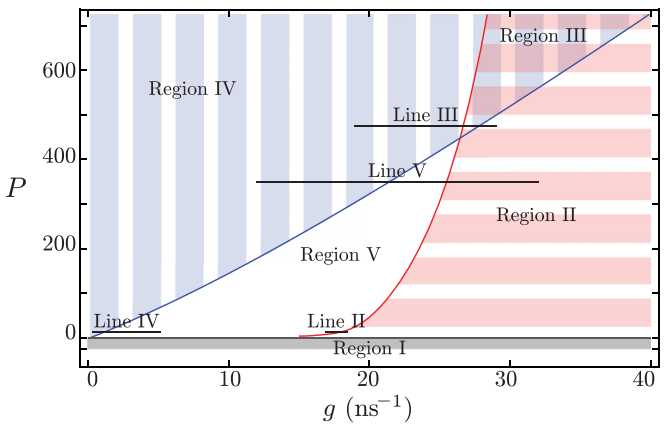

FIG. 1. Fixed-point classification from the stability analysis of a class-B laser coupled to a neutral resonator. Region I (gray) is a nonlasing region where the pump parameter lies below its threshold, $P < P_{\text{th}}$. In region II (red with horizontal stripes), the first fixed point is a saddle point and the second is a stable sink or stable spiral sink. Region IV (blue with vertical stripes) is the opposite. In region III (overlap), both fixed points are stable sinks or stable spiral sinks. In region V (white), both fixed points are saddle points and we find chaos in it and near its boundaries with region II and region IV.

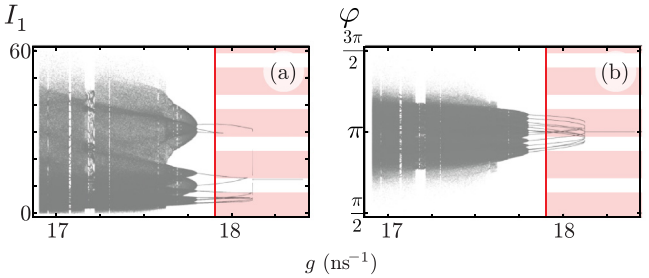

FIG. 2. Bifurcation diagrams for (a) twice the squared absolute value of the field amplitude I_1 and (b) phase difference between the field amplitudes φ for fixed pump parameter above threshold and variable coupling strength following line II in Fig. 1. The coloring matches that of regions in Fig. 1.

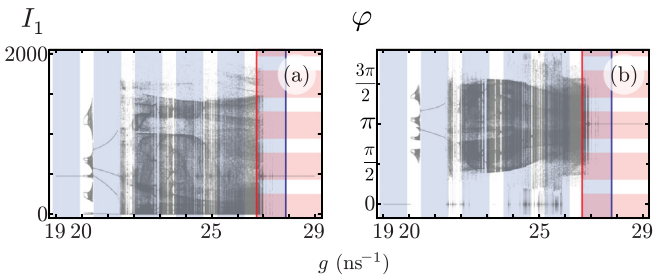

FIG. 3. Same as Fig. 2 but following line III in Fig. 1.

A. Region I

The pump parameter of the semiconductor laser is below its threshold value P_{th} and no lasing occurs, so both fields in the resonators deplete. At either fixed point, twice the squared absolute value of the amplitudes $I_1^{(j)}$ and $I_2^{(j)}$ is negative and therefore the fixed points are unphysical. The eigenvalues of the Jacobian evaluated on these fixed points predict saddle-point dynamics near them. This case is similar to a single class-B laser pumped below threshold. The system evolves to zero-field amplitudes and the carrier parameter to a negative value $N = P$ smaller than the stable carrier parameter for a single class-B laser pumped above threshold.

B. Region II

From this region forward, the two fixed points have identical nonzero amplitude, but their phase difference is zero, $\varphi^{(1)} = 0$, at the first fixed point and half a cycle, $\varphi^{(2)} = \pi$, at the second one. This region corresponds to large coupling strengths. Here, the first fixed point produces saddle dynamics and the second one produces stable sink dynamics, either spiral or nonspiral depending on the parameter values. In other words, we expect stable lasing as the fields reach steady state and their phase difference locks into a value of π. Region II shares a boundary with region V and region III on its left. Near these boundaries, we observe competition between the attractive component of the saddle point (fixed point 1) and the stable sink (fixed point 2). This produces a crossover from stability to multistability and eventually to chaos (Fig. 2) as the coupling strength g decreases while the pump parameter above threshold is kept constant (see line II in Fig. 1). This transition from chaos to a stable fixed point corresponds to a Hopf bifurcation for the second fixed point. There, the real part of a pair of eigenvalues of the Jacobian goes from positive to negative as the coupling strength g decreases. The multiple lines in the red region of Fig. 2 may arise due to limit cycles that are associated with Hopf bifurcations.

C. Region III

Region III appears for large values of the pump parameter above threshold, $P \gtrsim 350$. Here, both fixed points have stable behavior either as spiral or nonspiral sinks such that trajectories sufficiently close to either one of them will be attracted and remain there. Region III lies between regions II and IV where just one of the fixed points is stable. We expect equal and stable absolute values for the amplitudes at the resonators, a stable carrier parameter, and a phase difference locked at either zero or π, depending on the initial conditions. For a fixed pump parameter above threshold, as the coupling strength g increases, we go from a region on the left where the first fixed point is stable, to a region in the center where both fixed points are stable, to a region on the right where the second fixed point is stable (line III in Fig. 1). In both the extreme left and extreme right of this line, we find the expected stable behavior with a stable squared absolute value of the field amplitudes and stable phase differences of zero and π on the left and right, respectively. However, as we approach the boundaries between region IV and region III, we observe multistability and chaos (Fig. 3) as a consequence of the competition between the attractive components of the fixed points. While stable behavior is expected in both regions II and IV because of the presence of just one stable fixed point, we find chaotic behavior in region IV. Chaotic behavior coexisting with one or more stable fixed points has been found before [37,38].

D. Region IV

This region corresponds to small coupling strength values. The first fixed point produces stable sink dynamics, both spiral or nonspiral depending on the value of the pump parameter above threshold, and the second one produces saddle dynamics. We expect stable lasing as the fields reach steady state and their phase difference locks to zero. Region IV shares a boundary with region III and region V on its right. Near these boundaries, we observe competition between the stable sink provided by the first fixed point and the attractive component of the saddle point due to the second fixed point. This produces a crossover from stability to multistability and to chaos (Fig. 4) as the coupling strength g increases with a constant pump parameter above threshold (see line IV in Fig. 1). This transition from a stable fixed point to chaos corresponds to a Hopf bifurcation for the first fixed point. There, the real parts of a pair of eigenvalues of the Jacobian go from negative to positive as the coupling strength g increases.

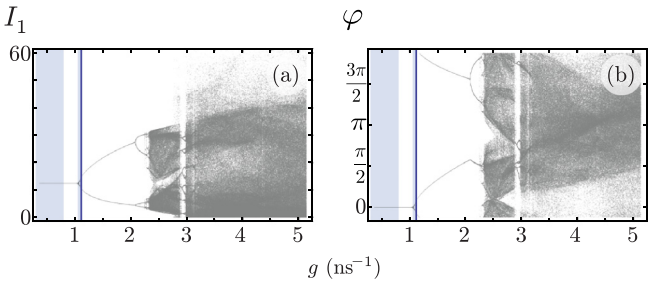

FIG. 4. Same as Fig. 2 but following line IV in Fig. 1.

E. Region V

This region exists for intermediate values of the coupling strength and relatively small values of the pump parameter above threshold, $P \lesssim 350$. Both fixed points present saddle dynamics. Competition between the attractive directions of the two saddle points leads to multistability and chaos. In this region both fixed points display saddle dynamics, meaning that neither is stable but both have attractive directions which pull trajectories. Region V shares a boundary on the right (left) with region II (region IV), where the second (first) fixed point is stable. For a fixed pump parameter above threshold, as the coupling strength g decreases (increases), the stability of the second (first) fixed point in region II (region IV) becomes multistable, eventually leading to chaos as we approach region V, Fig. 1 and line II (line IV) in Fig. 2 (Fig. 4). Figure 5 displays the full transition from region IV through region V and into region II for initial conditions nearby the first (second) fixed point with zero (π) phase difference, Figs. 5(a) and 5(b) [Figs. 5(c) and 5(d)]. For a fixed pump parameter above threshold, as the coupling strength increases, we go from a single attractive first fixed point on the left to a region where neither fixed points is attractive, in the center, to a single attractive second fixed point on the right. At the extreme left of this line, we find stable lasing and the phase difference φ locks to zero. As we approach the boundary with region V, multistability and chaos arise. In the center of the line, we observe chaotic behavior. Finally, on the extreme right of the line, we find stable lasing and the phase difference φ locks to a value of π. We want to stress that the system shows unstable behavior in the parameter regions where at least one fixed point is attractive (Fig. 5). This is to be expected. The stability analysis at fixed points is local and only implies that nearby trajectories get pulled to attractive fixed points. Therefore, whether a trajectory gets pulled or not depends on the initial conditions.

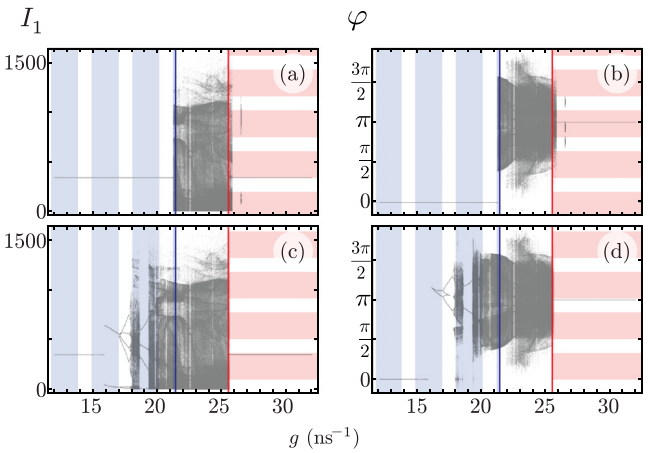

FIG. 5. Same as Fig. 2 but following line V in Fig. 1. The first (second) row displays initial conditions nearby the fixed point with zero (π) phase difference.

V. CONCLUSION

We studied a class-B laser resonator coupled to a neutral one and find a parameter space phase diagram showing a range of dynamical behaviors including phase-locked stable lasing, multistability, and chaos. This system may serve as a building block for larger arrays of coupled semiconductor lasers; it may be particularly useful for arrays requiring effective gain-loss dimers. Our basic dimer shows a rich dynamical landscape where sufficient control of the parameters in the system allows exploring stability with phase locking, multistability, and chaos.

For typical parameters of the class-B laser, we identified five regions in the parameter space phase diagram for zero detuning between the resonators. These regions are defined by the characteristics of the two fixed points from the system dynamics and controlled by the values of the pump parameter above threshold of the laser and coupling strength between resonators. In the first region, there is no lasing and the resonators are depleted but transient dynamics near the two fixed points shows an unstable phase difference. In the second and fourth regions, one fixed point is a stable sink and the other is a saddle point, leading to stable lasing with an equal squared absolute value of the field amplitudes and phase difference locked to π and zero, in that order, independently of the initial conditions. For any given initial condition in the second (fourth) region with large (small) coupling strength values, we are more likely to find stable lasing with the phase difference locked to a value of π (zero). For large values of the pump parameter above threshold, there is a region, the third one, with two attractive fixed points, where the phase difference locks to zero or π values depending on the initial conditions. In the fifth region, we are more likely to find multistable lasing and chaos. The transition from stable lasing to chaotic lasing is a crossover occurring in the boundaries between the second and the fifth regions and the fourth and the fifth regions.

In this work, for some initial configurations, we find unstable, multistable, and chaotic behavior for parameter values where at least one fixed point is stable. While this may seem counterintuitive, it is not forbidden. Cases of chaos coexisting with one or more stable fixed points have been reported before [37,38]. We want to stress that the stability analysis is local, i.e., it focuses the evolution of time-dependent quantities close to the fixed point. In consequence, the existence of an attractive fixed point only guarantees the stability of trajectories that start sufficiently close to it. For the same system, with the same pump rate, coupling, and laser parameters there could be unstable trajectories that do not start sufficiently close

to the attractive fixed point. In our system, we observe this chaotic behavior and multistability in the presence of one or two attractive fixed points for some trajectories that do not begin sufficiently close to these fixed points.

ACKNOWLEDGMENT

B.R.J.-Á. acknowledges financial support from Catedras CONACYT fellowship program 551.

[1] P. L. Gourley, M. E. Warren, G. R. Hadley, G. A. Vawter, T. M. Brennan, and B. E. Hammons, Coherent beams from high efficiency two-dimensional surface-emitting semiconductor laser arrays, Appl. Phys. Lett. **58**, 890 (1991).

[2] J. García-Ojalvo, J. Casademont, M. C. Torrent, C. R. Mirasso, and J. M. Sancho, Coherence and synchronization in diode-laser arrays with delayed global coupling, Int. J. Bifurcation Chaos **09**, 2225 (1999).

[3] M. A. Bandres, S. Wittek, G. Harari, M. Parto, J. Ren, M. Segev, D. N. Christodoulides, and M. Khajavikhan, Topological insulator laser: Experiments, Science **359**, eaar4005 (2018).

[4] G. Harari, M. A. Bandres, Y. Lumer, M. C. Rechtsman, Y. D. Chong, M. Khajavikhan, D. N. Christodoulides, and M. Segev, Topological insulator laser: Theory, Science **359**, eaar4003 (2018).

[5] S. Longhi, Y. Kominis, and V. Kovanis, Presence of temporal dynamical instabilities in topological insulator lasers, Europhys. Lett. **122**, 14004 (2018).

[6] M. Parto, S. Wittek, H. Hodaei, G. Harari, M. A. Bandres, J. Ren, M. C. Rechtsman, M. Segev, D. N. Christodoulides, and M. Khajavikhan, Edge-Mode Lasing in 1D Topological Active Arrays, Phys. Rev. Lett. **120**, 113901 (2018).

[7] H. Zhao, P. Miao, M. H. Teimourpour, S. Malzard, R. El-Ganainy, H. Schomerus, and L. Feng, Topological hybrid silicon microlasers, Nat. Commun. **9**, 981 (2018).

[8] A. Argyris, D. Syvridis, L. Larger, V. Annovazzi-Lodi, P. Colet, I. Fischer, J. García-Ojalvo, C. R. Mirasso, L. Pesquera, and K. A. Shore, Chaos-based communications at high bit rates using commercial fibre-optic links, Nature (London) **438**, 343 (2005).

[9] A. Uchida, *Optical Communication with Chaotic Lasers: Applications of Nonlinear Dynamics and Synchronization* (Wiley, New York, 2012).

[10] M. Sciamanna and K. A. Shore, Physics and applications of laser diode chaos, Nat. Photonics **9**, 151 (2015).

[11] S. Liu, N. Jiang, A. Zhao, Y. Zhang, and K. Qiu, Secure optical communication based on cluster chaos synchronization in semiconductor lasers network, IEEE Access **8**, 11872 (2020).

[12] S. Liu, N. Jiang, A. Zhao, Y. Zhang, and K. Qiu, Chaos synchronization and communication in global semiconductor laser network with coupling time delay signature concealment, Appl. Opt. **59**, 6788 (2020).

[13] S. Wieczorek, B. Krauskopf, T. B. Simpson, and D. Lenstra, The dynamical complexity of optically injected semiconductor lasers, Phys. Rep. **416**, 1 (2005).

[14] G. Baili, M. Alouini, T. Malherbe, D. Dolfi, I. Sagnes, and F. Bretenaker, Direct observation of the class-B to class-A transition in the dynamical behavior of a semiconductor laser, Europhys. Lett. **87**, 44005 (2009).

[15] F. T. Arecchi, G. L. Lippi, G. P. Puccioni, and J. R. Tredicce, Deterministic chaos in laser with injected signal, Opt. Commun. **51**, 308 (1984).

[16] H. G. Winful and S. S. Wang, Stability of phase locking in coupled semiconductor laser arrays, Appl. Phys. Lett. **53**, 1894 (1988).

[17] H. G. Winful and L. Rahman, Synchronized Chaos and Spatiotemporal Chaos in Arrays of Coupled Lasers, Phys. Rev. Lett. **65**, 1575 (1990).

[18] L. Zhang, W. Pan, L. Yan, B. Luo, X. Zou, and M. Xu, Cluster synchronization of coupled semiconductor lasers network with complex topology, IEEE J. Sel. Top. Quantum Electron. **25**, 1 (2019).

[19] L. Larger, B. Penkovsky, and Y. Maistrenko, Laser chimeras as a paradigm for multistable patterns in complex systems, Nat. Commun. **6**, 7752 (2015).

[20] J. Shena, J. Hizanidis, V. Kovanis, and G. P. Tsironis, Turbulent chimeras in large semiconductor laser arrays, Sci. Rep. **7**, 42116 (2017).

[21] A. Hohl, A. Gavrielides, T. Erneux, and V. Kovanis, Localized Synchronization in Two Coupled Nonidentical Semiconductor Lasers, Phys. Rev. Lett. **78**, 4745 (1997).

[22] Y. Kominis, V. Kovanis, and T. Bountis, Spectral signatures of exceptional points and bifurcations in the fundamental active photonic dimer, Phys. Rev. A **96**, 053837 (2017).

[23] Y. Kominis, A. Bountis, and V. Kovanis, Radically tunable ultrafast photonic oscillators via differential pumping, J. Appl. Phys. **127**, 083103 (2020).

[24] Y. Kominis, V. Kovanis, and T. Bountis, Controllable asymmetric phase-locked states of the fundamental active photonic dimer, Phys. Rev. A **96**, 043836 (2017).

[25] T. Erneux and D. Lenstra, Synchronization of mutually delay-coupled quantum cascade lasers with distinct pump strengths, Photonics **6**, 125 (2019).

[26] F. M. Dubois, M. Seifikar, A. H. Perrott, and F. H. Peters, Modeling mutually coupled non-identical semiconductor lasers on photonic integrated circuits, Appl. Opt. **57**, E154 (2018).

[27] Z. Gao, M. T. Johnson, and K. D. Choquette, Rate equation analysis and non-hermiticity in coupled semiconductor laser arrays, J. Appl. Phys. **123**, 173102 (2018).

[28] M. Adams, R. A. Seyab, I. Henning, H. Susanto, and M. Vaughan, Dynamics of evanescently-coupled laser pairs with unequal pumping: Analysis using a three-variable reduction of the coupled rate equations, IEEE J. Sel. Top. Quantum Electron. **28**, 1 (2022).

[29] A. Padrón-Godínez, B. Jaramillo-Ávila, and B. M. Rodríguez-Lara, Lasing in para-Fermi class-B microring resonator arrays, Phys. Rev. A **102**, 023511 (2020).

[30] D. Pieroux, T. Erneux, and K. Otsuka, Minimal model of a class-B laser with delayed feedback: Cascading branching of periodic solutions and period-doubling bifurcation, Phys. Rev. A **50**, 1822 (1994).

[31] S.-S. Li, Q. Liu, and S.-C. Chan, Distributed feedbacks for time-delay signature suppression of chaos generated from a semiconductor laser, IEEE Photonics J. **4**, 1930 (2012).

[32] T. Erneux and P. Glorieux, *Laser Dynamics* (Cambridge University Press, Cambridge, UK, 2010).

[33] J. Guckenheimer and P. Holmes, *Nonlinear Ordinary Differential Equations* (Springer, New York, 1983).

[34] D. Jordan and P. Smith, *Nonlinear Ordinary Differential Equations* (Oxford University Press, Oxford U.K., 2007).

[35] B. E. Little, S. T. Chu, H. A. Haus, J. Foresi, and J.-P. Laine, Microring resonator channel dropping filters, J. Lightwave Technol. **15**, 998 (1997).

[36] Y. Liu, T. Chang, and A. E. Craig, Coupled mode theory for modeling microring resonators, Opt. Eng. **44**, 084601 (2005).

[37] X. Wang and G. Chen, A chaotic system with only one stable equilibrium, Commun. Nonlinear Sci. Numer. Simul. **17**, 1264 (2012).

[38] J. C. Sprott, X. Wang, and G. Chen, Coexistence of point, periodic and strange attractors, Int. J. Bifurcation Chaos **23**, 1350093 (2013).